High energy resolution x-ray absorption spectroscopy study of uranium in varying valence states

T. Vitova,[1,*] K. O. Kvashnina,[2,†] G. Nocton,[3] G. Sukharina,[4] M. A. Denecke,[1] S. M. Butorin,[5] M. Mazzanti,[3] R. Caciuffo,[6] A. Soldatov,[4] T. Behrends,[7] and H. Geckeis[1]

[1]*Institute for Nuclear Waste Disposal (INE), Karlsruhe Institute of Technology, P.O. Box 3640, D-76021 Karlsruhe, Germany*

[2]*European Synchrotron Radiation Facility (ESRF), 6 Rue Jules Horowitz, BP 220, 38043 Grenoble Cedex 9, France*

[3]*Laboratoire de Reconnaissance Ionique et Chimie de Coordination, SCIB (UMR-E 3 CEA-UJF), INAC, CEA-Grenoble, 17 rue des Martyrs, 38054 Grenoble Cedex 09, France*

[4]*Faculty of Physics, Southern Federal University, Rostov-on-Don 344090, Russia*

[5]*Department of Physics, Uppsala University, P.O. Box 530, SE-751 21 Uppsala, Sweden*

[6]*Institute for Transuranium Elements (ITU), Joint Research Centre, European Commission, P.O. Box 2340, D-76125 Karlsruhe, Germany*

[7]*Faculty of Geosciences, Utrecht University, P.O. Box 80021, NL-3508 Utrecht, The Netherlands*

(Received 21 July 2010; published 14 December 2010)

A high energy resolution x-ray absorption near-edge structure (XANES) spectroscopy study on U^{4+} (UO_2), U^{5+} ($[UO_2Py_5][KI_2Py_2]$), and U^{6+} $[UO_2(NO_3)_2(H_2O)_6]$ demonstrates the potential of this experimental technique for qualitative/semiqualitative and quantitative actinide speciation investigations. We observe a pre-edge feature with quadrupole nature in a U L_3 edge partial fluorescence yield-XANES spectrum. This feature is a tool for characterizing the participation of $5f$ orbitals in U-O bonding. The feature origin is explained by performing calculations with the finite difference method near-edge structure code based on the multiple-scattering theory and the finite difference method.

DOI: 10.1103/PhysRevB.82.235118 PACS number(s): 78.70.Dm, 61.05.cj, 71.20.−b, 78.70.En

I. INTRODUCTION

The complexity of the chemistry and physics of actinide elements (An) requires development and application of experimental techniques that provide, supported by theoretical calculations, a deeper insight into the structure and reactivity of these elements on an atomic/molecular scale. This knowledge is prerequisite for controlling and predicting An reactivity, which is the major challenge in ensuring long term safe disposal of high-level radioactive waste and in efforts to reduce the radiotoxicity of spent nuclear fuel. X-ray absorption spectroscopy measured at energies near the ionization energy, i.e., x-ray absorption near-edge structure (XANES) regime, has become a widely established method for An oxidation state characterization,[1,2] addressing scientific cases such as interaction of An with the biosphere,[3] formation and transport of An containing colloids in the environment,[4] solution An chemistry,[5] sorption/desorption processes on mineral-water interfaces,[6] and partitioning or the separation of An cations from their chemically similar lanthanide homologs.[7] The An elements, especially Pu, frequently occur in various oxidation states in the same system and determination of An valence is often challenging. XANES in fluorescence mode is often the only applicable characterization technique, as it has no limitation with respect to the probed element, requires no special sample preparation which might inadvertently alter the An speciation and is a bulk, commonly nondestructive technique. Furthermore, for radioactive An samples, radiation protection containments for *in situ* experiments do not interfere due to the high-penetration depth of the high photon energies at An L_3 absorption edges (16.3 to 19.9 keV for Th to Cf). Finally, XANES can be applied for a selected element with low concentration in solid, liquid, or gaseous phase systems. The partial fluorescence yield technique-XANES (PFY-XANES) underwent a rapid development during the past 5 years (see, e.g., Refs. 8–10). However, its potential for advanced investigations of An electronic properties/valence states and An atomic environment has not yet been explicitly demonstrated. To our knowledge, only one peer reviewed study on L_3 edge PFY-XANES of actinide materials exists.[11] We report a spectroscopic observation of a pre-edge structure in U L_3 edge PFY-XANES spectra with quadrupole nature, which is extremely valuable for quantification of the degree of $5f$ orbital participation in U-O bonding. PFY-XANES spectra of U^{4+}, U^{5+}, and U^{6+} materials, supported by theoretical calculations based on the multiple-scattering code and the finite difference method [finite difference method near-edge structure (FDMNES) code[12]] are discussed. The inherent greater sensitivity of PFY-XANES to changes in valence states and atomic environment over conventional XANES is comprehensively demonstrated and thereby serves to motivate its implementation for investigations relevant to An material science and chemistry.

The inherent improvement in energy resolution of a PFY-XANES experiment lies in partly overcoming core-hole lifetime broadening effects.[13–15] For example, the PFY-XANES spectra in Fig. 2 correspond to diagonal section (solid lines) through the X-emission planes in Figs. 1(a)–1(c) at the maximum of the U $L\alpha_1$ emission line. In contrast, the total x-ray emission signal in the planes is integrated to obtain the total fluorescence yield-XANES (TFY-XANES) spectra (see Fig. 2). The energy resolution of a XANES spectrum depends generally on the experimental energy resolution and the core-hole lifetime broadening in the final state.[13,14] In a standard transmission mode An L_3 edge XANES experiment, the $2p_{3/2}$ core-hole lifetime broadening is 7.1–8.8 eV (Th to Cf).[16] A spectral narrowing below the natural core-hole lifetime width is achieved by employing an x-ray emission spectrometer.[15] The spectrometer is tuned to the $L\alpha_1$ ($3d_{5/2}$-$2p_{3/2}$) fluorescence line and the absorption is recorded by monitoring the $L\alpha_1$ intensity as a function of the incident energy. In that case the width of the spectral features is no longer limited by the $2p_{3/2}$ core-hole lifetime but by the

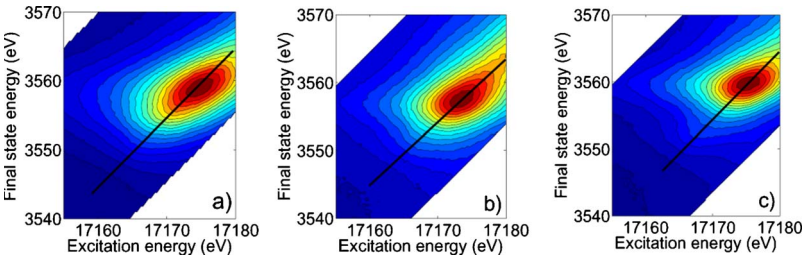

FIG. 1. (Color online) (a) U $L\alpha_1$ emission of UO_2 (U^{4+}), (b) $[UO_2Py_5][KI_2Py_2]$ (U^{5+}), and (c) $UO_2(NO_3)_2(H_2O)_6$ (U^{6+}) plotted on the final-state energy scale (final-state energy = excitation energy − emission energy) as a function of the excitation energy.

sharper $3d_{5/2}$ core-hole width (4 eV) in the final state.[17] The advantage of recording measurements with about half the natural linewidth, however, is not exploited in a standard fluorescence experiment, as the energy resolution of a solid-state fluorescence detector, normally used, is greater than 100 eV, thereby limiting the overall spectral energy resolution. The ability and advantage of PFY-XANES was first demonstrated in 1991.[13]

II. EXPERIMENT, METHODS, AND DATA EVALUATION

PFY-XANES experiments were performed at the beamline ID26 at the European Synchrotron Radiation Facility (ESRF) in Grenoble. The incident energy was selected using the (311) reflection of a double Si crystal monochromator. Rejection of higher harmonics was achieved by three Pd/Cr mirrors working under total reflection. The energy calibration was performed using a Zr foil (17998 eV). The incident x-ray beam had a flux of approximately 2×10^{13} photons/s at the sample position. The emission energy was selected using the (777) reflection of a spherically bent Ge crystal analyzer (bending radius $R=1$ m) aligned at 77° Bragg angle. A combined (incident convoluted with emitted) energy resolution of 2.5 eV was estimated. XANES spectra were measured simultaneously in PFY-XANES mode using the x-ray emission spectrometer[15] and TFY-XANES using an avalanche photodiode. The energy of the incident beam was scanned from 17151.2 to 17225.2 eV, in 0.1 eV steps, over the U L_3 absorption edge (ionization energy for U^0 = 17 166 eV). The UO_2 sample was in a single-crystal form, whereas $[UO_2Py_5][KI_2Py_2]$ (Py stands for pyridine, C_5H_5N) and $[UO_2(NO_3)_2(H_2O)_6]$ samples were prepared as pressed pellets. In the $[UO_2Py_5][KI_2Py_2]$ sample, the U ions are in the pentavalent state and are redox sensitive. This particular sample was kept in Ar atmosphere and cooled by a cryostream system in order to prevent chemical state changes. The $[UO_2Py_5][KI_2Py_2]$ sample showed radiation damage after exposure times longer than 60 s, therefore, spectra were recorded for 30 s and repeated at different pristine positions on the sample. The UO_2 and $UO_2(NO_3)_2(H_2O)_6$ samples showed no radiation damage during the experiment. No polarization-dependent effects were observed on the UO_2 PFY-XANES spectra measured with a 90°, 45°, and 0° orientation between the UO_2 single-crystal face and the polarization vector of the incoming beam.

The FDMNES (Ref. 12) calculations were performed using an atomic cluster with radius 4.6 Å for UO_2, 4.6 Å for $[UO_2Py_5][KI_2Py_2]$, and 6.2 Å for $UO_2(NO_3)_2(H_2O)_6$ using Cartesian coordinates listed in the Inorganic Crystal Structure Database (ICSD) files given below. For the $UO_2(NO_3)_2(H_2O)_6$ compound we used a larger cluster size because the more layered structure requires taking more distant atoms into account to obtain reliable XANES spectra. As large space simulations demand extremely large computer resources, we used smaller clusters for more condensed materials. The FDMNES input file applied for the calculations of the U^{6+} L_3 edge XANES and the angular momentum projected density-of-states spectra can be seen in the supplementary materials.[18] Relativistic self-consistent field calculations using Dirac-Slater approach have been performed for each nonequivalent atom in the considered cluster. From the superposed self-consistent atomic densities in the selected cluster of atoms, the Poisson equation was solved to obtain the Coulomb potential. The energy-dependent exchange-correlation potential was evaluated using the local-density approximation. Exchange-correlation potential was constructed using real Hedin-Lundquist and Von Barth formulation. Calculations were performed with and without consideration of $2p_{3/2}\rightarrow5f$ transitions and no experimental broadening was included. Polarization dependency was not included in the calculation of the UO_2 spectrum.

The linear combination least-squares fit modeling of the TFY/PFY-XANES U^{4+}, U^{5+}, and U^{6+} spectra was performed with the WINXAS program[19] (www.winxas.de) utilizing three pseudo-Voigt (P.V.) $[f(x)=\alpha\text{Gaussian}+(1-\alpha)\text{Lorentzian}]$ and one arctangent line shapes. The Levenberg-Marquardt

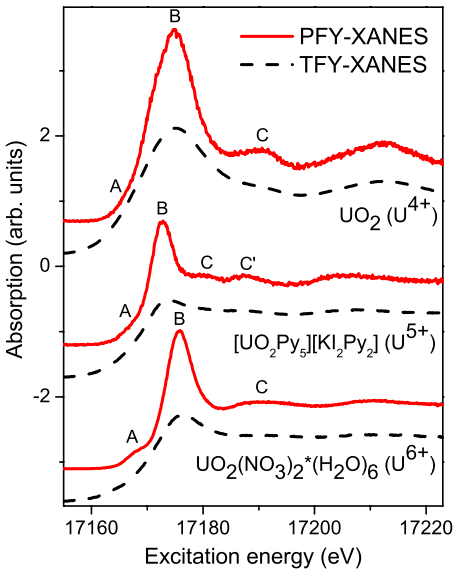

FIG. 2. (Color online) The U L_3 edge PFY-XANES and TFY-XANES spectra of UO_2 (U^{4+}), $[UO_2Py_5][KI_2Py_2]$ (U^{5+}), and $UO_2(NO_3)_2(H_2O)_6$ (U^{6+}).

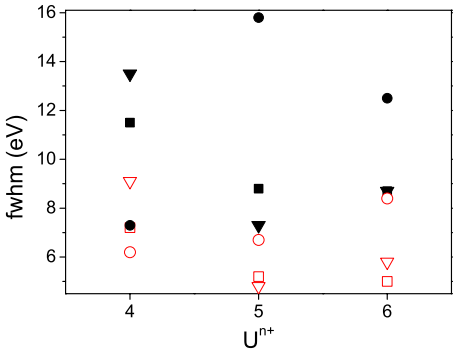

FIG. 3. (Color online) The fwhm values of the A, B, C resonant features in the PFY-XANES and TFY-XANES spectra displayed in Fig. 1. Open (closed) symbols refer to PFY (TFY)-XANES spectra; (square) A feature; (triangle) B feature; and (circle) C feature.

least-squares algorithm is used in the fit. Please see details of the algorithm in Ref. 20.

III. RESULTS AND DISCUSSION

A. Studied materials

UO_2 is a semiconductor with cubic fluorite ($Fm\bar{3}m$, a =5.4682 Å) structure and $5f^2$ (U^{4+}) valence configuration. The U atoms are surrounded by eight O atoms at 2.3678 Å distance (ICSD 35204). The $[UO_2Py_5][KI_2Py_2]$ and $UO_2(NO_3)_2(H_2O)_6$ have monoclinic ($P12_1/m$ 1) (Ref. 21) and orthorhombic ($Cmc21$, ICSD 23825) crystal structures and $5f^1$ and $5f^0$ valence configurations, respectively. In both systems, two O atoms are bond to the U atoms in a linear fashion in the axial plane, building the well-known uranyl moiety $[UO_2]^+/[UO_2]^{2+}$. The short U-O axial bond (one O atom at 1.83 and the other at 1.84 Å in the U^{5+} compound, and one O at 1.75 Å and one O at 1.77 Å in the U^{6+} compound) is a common structural feature for early An^{5+} and An^{6+} (U-Pu) solid oxide materials and aqueous solutions.[1,2] The uranium coordination polyhedron in $[UO_2Py_5][KI_2Py_2]$ and $UO_2(NO_3)_2(H_2O)_6$ is completed by five N (U^{5+}) atoms located at 2.601–2.612 Å interatomic distances in the equatorial plane and six O (U^{6+}) atoms at 2.397–2.548 Å, respectively.

B. Experimental results

The U L_3 edge TFY-XANES and PFY-XANES spectra of the three measured samples are shown in Fig. 2 and the full width at half maximum (fwhm) values determined for the resonant features A, B, and C are shown in Fig. 3 (see also Table I). The spectral features of the PFY-XANES spectra in Fig. 2 have significantly smaller fwhm values, ranging from 5 to approximately 9 eV, compared to the simultaneously measured conventional TFY spectra (fwhm values from 7.3 eV to nearly 16 eV) and therefore, are better energy resolved. The most intense resonance B [white line (WL)] partially describing dipole allowed U $2p_{3/2} \rightarrow 6d$ electronic transitions[22,23] is sharp and well separated from the C structure in the PFY-XANES spectra but not in the TFY-XANES. The A resonance in the pre-edge region of the PFY-XANES spectra is observed here in an actinide L_3 edge XANES (cf. the discussion below). It must be noticed that this feature is clearly visible in the U^{6+} case and only partially visible in the U^{5+} case. On the contrary, in the U^{4+} PFY-XANES spectrum it overlaps with the WL and is therefore hidden (see Table I and Fig. 4). The structures above 17 200 eV are due to scattering of the photoelectron from the surrounding atoms. These features are intrinsically broad; therefore this advanced spectroscopy here does not provide new information. A common approach in detection of An minority valence species in oxidation state mixtures is to compare the WL or edge jump energy positions (fingerprinting) of the spectrum of the investigated compound with those observed in reference compounds. The proportion of species in mixtures is often determined by performing linear combination least-squares fit analyses using XANES spectra of suitable An reference materials. However, all three conventional U L_3 edge XANES spectra in Fig. 2 are dominated by broad features, the differences in their edge energies are small, their energy positions "unconventional" and the fine structure rather featureless, so that oxidation state and species determinations are difficult. The TFY-XANES U^{5+} and U^{6+} spectra have a similar spectral appearance having both short-axial U-O bonds. The resonance appearing as a shoulder on the high energy flank of the WL originates from multiple scattering of the $2p_{3/2}$ photoelectron along the two axial O atoms.[24,25] Its energy position depends on the U-O distance, which can vary between compounds with same valence but different constituents in the equatorial bonding plane by 0.2 Å from U to Am.[1,2] Additional difficulty in the analysis of XANES lies in the WL energy positions of the U^{5+} and U^{6+} TFY-XANES. These are at lower and slightly higher energy positions, respectively (see Fig. 2 and Table I), compared to the U^{4+} TFY-XANES WL maximum,[23] which contradicts the general expectation of WL maxima shifting to higher energy with increasing oxidation state.[25] This effect is explained by the extremely short U-O uranyl axial bond, leading to strong mixing of the U $6d$ and O $2p$ orbitals and thereby introducing covalent bond character.[22] As a result, the U^{5+}/U^{6+} $6d$ states are pulled to lower energies compared to the U^{4+} $6d$ states. The structural peculiarity of the uranyl cation also explains the lower U^{5+} and U^{6+} WL amplitudes compared to the U^{4+} WL in the frame of multiple-scattering theory.[25] Note that, this situation changes for the L_3 edge XANES spectra of the few An^{5+} and An^{6+} oxide materials reported not having the short An-O bond (see, e.g., Ref. 26). Variation in the WL intensity can also be influenced by other factors such as, solid-state condensation effects.[5] The difficulties in An XANES speciation characterization discussed above can be overcome by utilizing the better energy resolved U L_3 edge PFY-XANES spectra in qualitative (fingerprinting) or semiqualitative (e.g., linear combination least-squares fit) analyses. The U L_3 edge PFY-XANES spectra are also favorable for quantitative analyses as they can be successfully calculated using theoretical codes.

C. Theoretical results

The experimental U^{4+}, U^{5+}, and U^{6+} PFY-XANES spectra are compared against those calculated by the FDMNES code in

TABLE I. Height, position, and fwhm parameters of the pseudo-Voigt functions used to model XANES resonance features (A, B, C for PFY-XANES/A_TFY, B_TFY, C_TFY for TFY-XANES) and the arctangent (atan/atan_TFY) function to model the edge jump (see Fig. 4), as well as the Gauss part (α) and the area of the P.V. The parameters were either fixed (f) or varied (v) during the fit.

U^{n+}	Resonance	Height ±0.01	Position ±0.02	fwhm ±0.01	α	Area
U^{4+}	A	0.27^{v}	17169.0^{f}	7.2^{v}	1.0^{v}	2.1
U^{4+}	A_TFY	0.13^{v}	17169.0^{f}	11.5^{v}	1.0^{v}	1.6
U^{5+}	A	0.26^{v}	17167.9^{f}	5.2^{v}	1.0^{v}	1.4
U^{5+}	A_TFY	0.20^{v}	17167.9^{f}	8.8^{v}	1.0^{v}	1.9
U^{6+}	A	0.22^{v}	17168.7^{f}	5.0^{v}	1.0^{v}	1.2
U^{6+}	A_TFY	0.20^{v}	17168.7^{f}	8.7^{v}	1.0^{v}	2.1
U^{4+}	B	2.76^{v}	17174.9^{f}	9.1^{v}	1.0^{v}	26.8
U^{4+}	B_TFY	1.70^{v}	17174.9^{f}	13.5^{v}	1.0^{v}	23.8
U^{5+}	B	1.76^{v}	17172.8^{f}	4.8^{v}	1.0^{v}	8.0
U^{5+}	B_TFY	0.80^{v}	17172.8^{f}	7.3^{v}	1.0^{v}	1.9
U^{6+}	B	2.01^{v}	17175.7^{f}	5.8^{v}	1.0^{v}	12.5
U^{6+}	B_TFY	1.10^{v}	17175.7^{f}	8.7^{v}	1.0^{v}	10.6
U^{4+}	C	0.14^{v}	17189.0^{f}	6.2^{v}	1.0^{v}	0.9
U^{4+}	C_TFY	0.13^{v}	17189.0^{f}	7.3^{v}	1.0^{v}	1.0
U^{5+}	C	0.15^{v}	17179.1^{f}	6.7^{v}	1.0^{v}	1.0
U^{5+}	C_TFY	0.10^{v}	17179.1^{f}	15.8^{v}	1.0^{v}	1.5
U^{6+}	C	0.06^{v}	17190.2^{f}	8.4^{v}	1.0^{v}	0.5
U^{6+}	C_TFY	0.06^{v}	17190.2^{f}	12.5^{v}	1.0^{v}	0.8
U^{4+}	atan	1.00^{f}	17181.0^{v}	5.0^{v}		13.7
U^{4+}	atan_TFY	1.00^{f}	17181.0^{f}	12.7^{v}		17.6
U^{5+}	atan	1.00^{f}	17175.7^{v}	3.4^{v}		9.2
U^{5+}	atan_TFY	1.00^{f}	17175.7^{f}	6.4^{v}		10.8
U^{6+}	atan	1.00^{f}	17179.0^{v}	4.1^{v}		21.6
U^{6+}	atan_TFY	1.00^{f}	17179.0^{f}	6.7^{v}		20.3

Figs. 5(a)–5(c). Calculations were performed with and without consideration of the $2p_{3/2} \rightarrow 5f$ transitions and no experimental broadening was included. All theoretical spectra in Fig. 5 reproduce the general shape and number of post-WL resonances in the PFY-XANES spectra. The resonances are shifted by less than 1 eV to lower energies with respect to the experimental energy positions. The theoretical U^{4+} WL is split into two energy levels, reflecting the splitting of the $6d$ band. This splitting is not resolved in our experiment but it is revealed by the asymmetric shape of the WL. The energy difference between the calculated $2p_{3/2} \rightarrow 5f$ [labeled in Fig. 5(c)] and the $2p_{3/2} \rightarrow 6d$ peaks is 5.5 eV for U^{4+}, 3 eV for U^{5+}, and 4.5 eV for the U^{6+} containing samples. The corresponding energy differences between resonance features A and B (Table I) are 5.9 eV, 4.9 eV, and 7 eV, respectively. Although the calculated values here differ by 0.4–2.5 eV from the experimental ones, the calculations follow the same trend, with U^{5+} showing the smallest energy difference and U^{6+} the largest. It must be noticed that the matrix element for the $p \rightarrow s$ channel is about two orders of magnitude smaller than for the $p \rightarrow d$ one; therefore nearly the $p \rightarrow d$ channel alone represents the overall spectral shape (see Figs. 5 and 6).

In $3d$ metals with inversion symmetry, the A pre-edge feature is attributed to pure quadrupole $1s \rightarrow 3d$ electronic transitions ($\Delta l = 0, \pm 2$). When lower symmetry occurs, the pre-edge gains additional intensity from dipole allowed transitions to states with p character ($\Delta l = \pm 1$).[9] Inversion symmetry is present only in the U^{4+} (O_h) material [U^{5+} (D_{5h}); U^{6+} (D_{3h})], whereas the U unoccupied angular momentum projected density of states (d/f-DOS) in Fig. 6 show mixing of U d and U f empty valence states on the rising absorption edge for U^{4+} and U^{5+}, and no mixing for U^{6+}. Despite the minor discrepancies between the FDMNES calculations and the experimental PFY-XANES, which might be attributed to the lack of many-body effects in the code, theory reproduces the experimental spectra reasonably well. This suggests that the pre-edge peak A, especially evident in the PFY-XANES U^{6+} spectrum, originates from $2p_{3/2} \rightarrow 5f$ electronic transitions. The feature intensity and the observed differences in pre-edge peak energy position indicate that it can be used for An oxidation state determination in a manner similar to that already used extensively in K-edge XANES speciation investigations of $3d$ and $4d$ metals using the $1s \rightarrow 3d$ and $1s \rightarrow 4d$ quadrupole transition energies and intensities.[8–10] However, this An L_3 pre-peak feature is expected to also be sensitive to additional factors affecting the electron density in the f-like final states such as changes in symmetry, type of axial and equatorial ligands and bonding character. Further study will reveal if insight into these factors for unknown

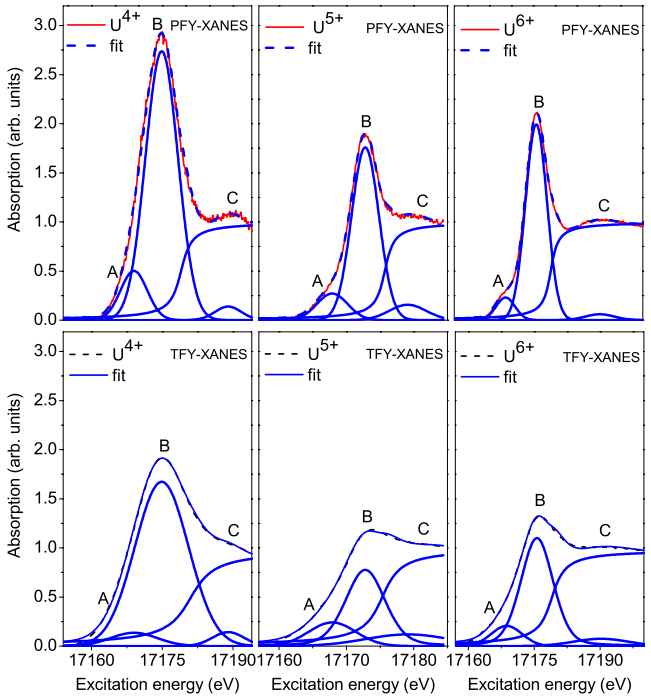

FIG. 4. (Color online) The U L_3 edge PFY-XANES (top row) and TFY-XANES (bottom row) spectra of UO_2 (U^{4+}), $[UO_2Py_5][KI_2Py_2]$ (U^{5+}), and $UO_2(NO_3)_2(H_2O)_6$ (U^{6+}). The pseudo-Voigt line shapes used in the linear combination analyses (see Table I).

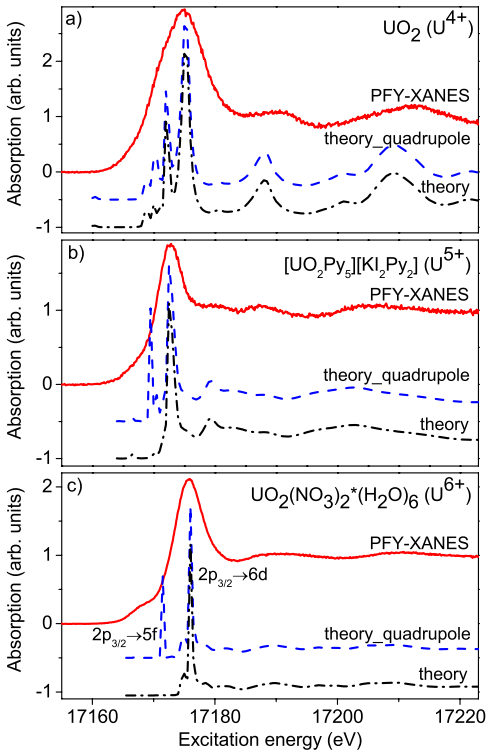

FIG. 5. (Color online) The U L_3 edge PFY-XANES spectra of (a) UO_2 (U^{4+}), (b) $[UO_2Py_5][KI_2Py_2]$ (U^{5+}), and (c) $UO_2(NO_3)_2(H_2O)_6$ (U^{6+}) compared to theoretical calculations (FDMNES) with (theory_quadrupole) and without (theory) $2p_{3/2} \rightarrow 5f$ electronic transitions.

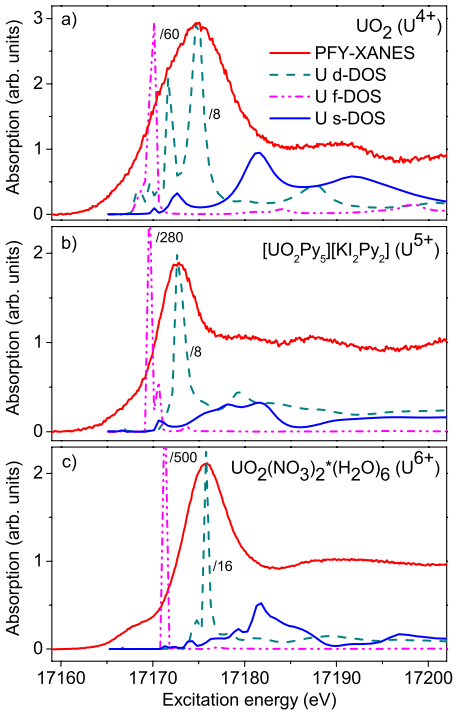

FIG. 6. (Color online) The U L_3 edge PFY-XANES spectra and the calculated (FDMNES) unoccupied U d-, U f- and U s-angular momentum projected $d/f/s$-DOS of (a) UO_2 (U^{4+}), (b) $[UO_2Py_5][KI_2Py_2]$ (U^{5+}), and (c) $UO_2(NO_3)_2(H_2O)_6$ (U^{6+}).

systems can be derived from analysis of this pre-edge feature.

IV. CONCLUSION

We report a pre-edge feature in an actinide L_3 edge XANES spectrum. The theoretical calculations (FDMNES code) indicate that this resonance originates from quadrupole $2p_{3/2} \rightarrow 5f$ electronic transitions. The still widely discussed question of the level of participation of the $5f$ orbitals in An-O bonding can be elucidated by comparing the oscillatory strength of this feature for different An oxide materials. The stronger the U $5f$-O $2p$ orbitals mixing, the higher the probability for ligand-metal charge-transfer potentially leading to reduced pre-edge amplitude and energy position shifts. The presented high energy resolution technique opens perspectives for extracting precise An electronic and coordination structure information. Distinct development in theoretical methods for precise calculation of PFY-XANES spectra to support these activities are highly desirable. Finally, we believe that our experimental and theoretical observation will stimulate more discussions about electronic structure of actinide systems, in general.

ACKNOWLEDGMENTS

We acknowledge P. Colomp and the ESRF radiation protection staff for assistance in handling the uranium samples, and the ID26 beamline staff for assistance during the experiment.

*tonya.vitova@kit.edu
†kristina.kvashnina@esrf.fr

[1] M. A. Denecke, Coord. Chem. Rev. **250**, 730 (2006).
[2] M. R. Antonio and L. Soderholm, *The Chemistry of the Actinides and Transactinide Elements* (Springer, New York, 1994), Vol. 5.
[3] A. Geissler, S. Selenska-Pobell, K. Morris, F. R. Livens, and J. R. Lloyd, *Ecology of Industrial Pollution* (Cambridge University, Cambridge, 2010).
[4] A. P. Novikov, S. N. Kalmykov, S. Utsunomiya, R. C. Ewing, F. Horreard, A. Merkulov, S. B. Clark, V. V. Tkachev, and B. F. Myasoedov, Science **314**, 638 (2006).
[5] C. Walther, J. Rothe, B. Brendebach, M. Fuss, M. Altmaier, C. M. Marquardt, S. Büchner, H.-R. Cho, J.-I. Yun, and A. Seibert, Radiochim. Acta **97**, 199 (2009).
[6] P. Martin, S. Grandjean, M. Ripert, M. Freyss, P. Blanc, and T. Petit, J. Nucl. Mater. **320**, 138 (2003).
[7] N. L. Banik, B. Schimmelpfennig, C. M. Marquardt, B. Brendebach, A. Geist, and M. A. Denecke, Dalton Trans. **39**, 5117 (2010).
[8] H. Hayashi, Anal. Sci. **24**, 15 (2008).
[9] F. de Groot, G. Vanko, and P. Glatzel, J. Phys.: Condens. Matter **21**, 104207 (2009).
[10] T. Vitova, J. Hormes, M. Falk, and K. Buse, J. Appl. Phys. **105**, 013524 (2009).
[11] J.-P. Rueff, S. Raymond, A. Yaresko, D. Braithwaite, Ph. Leininger, G. Vankó, A. Huxley, J. Rebizant, and N. Sato, Phys. Rev. B **76**, 085113 (2007).
[12] Y. Joly, Phys. Rev. B **63**, 125120 (2001).
[13] K. Hämäläinen, D. P. Siddons, J. B. Hastings, and L. E. Berman, Phys. Rev. Lett. **67**, 2850 (1991).
[14] F. M. F. de Groot and A. Kotani, *Core Level Spectroscopy of Solids* (Taylor & Francis, London, 2008).
[15] P. Glatzel and U. Bergmann, Coord. Chem. Rev. **249**, 65 (2005).
[16] M. O. Krause and J. H. Oliver, J. Phys. Chem. Ref. Data **8**, 329 (1979).
[17] O. Keski-Rahkonen and M. O. Krause, Phys. Rev. A **15**, 959 (1977).
[18] See supplementary material at http://link.aps.org/supplemental/10.1103/PhysRevB.82.235118 for an example of a FDMNES input file used in the calculations.
[19] T. Ressler, J. Synchrotron Radiat. **5**, 118 (1998).
[20] W. H. Press, B. P. Flannery, S. A. Teukolsky, and W. T. Vetterling, *Numerical Recipes in C* (Cambridge University, Cambridge, 1989).
[21] L. Natrajan, F. Burdet, J. Pécaut, and M. Mazzanti, J. Am. Chem. Soc. **128**, 7152 (2006).
[22] R. G. Denning, J. Phys. Chem. A **111**, 4125 (2007).
[23] C. DenAuwer, E. Simoni, S. Conradson, and C. Madic, Eur. J. Inorg. Chem. **2003**, 3843 (2003).
[24] E. A. Hudson, P. G. Allen, L. J. Terminello, M. A. Denecke, and T. Reich, Phys. Rev. B **54**, 156 (1996).
[25] A. L. Ankudinov, S. D. Conradson, J. Mustre de Leon, and J. J. Rehr, Phys. Rev. B **57**, 7518 (1998).
[26] A. V. Soldatov, D. Lamoen, M. J. Konstantinovic, S. V. den Berghe, A. C. Scheinost, and M. Verwerft, J. Solid State Chem. **180**, 54 (2007).